Stereoscopic Camera-Based Investigation of Pulverized Solid Fuel Combustion - particle temperature, shape and burning rates

M. Schiemann*[1], N. Vorobiev[1]

[1]Ruhr-University, Bochum, Germany

Abstract

A newly developed stereoscopic camera system has been applied to measure the temperature, size and shape of burning coal and biomass particles in a lab-scale laminar flow reactor. The stereoscopic imaging method enables to measure the particle contour which can be used to determine the shape of the particle. As the camera system is constructed for two-color pyrometry, the simultaneous detection of the particle temperature is possible and provides data which can be used to calculate char burning rate parameters. Initial results are shown for biomass combustion, with measurements carried out in a O_2/N_2 atmosphere.

Introduction

The determination of char burning rate parameters is an important issue when the combustion properties of pulverized fuels (pf, d_p~ 100 µm) are investigated. As char combustion is slow compared to the combustion of volatiles released during the pyrolysis phase, its profound knowledge is important to predict fuel conversion and thus heat release precisely when designing pf-boilers.

Ratio pyrometry is a common technique for the investigation of char combustion. It is contactless and due to the high sensitivity of modern detectors, allows to measure particle temperature and size of pf-particles suspended in gas flows under realistic boundary conditions. It has to be distinguished between non-imaging or point detectors and imaging devices. Point detectors (e.g. PMTs) have been used in different setups. The determination of burning rate parameters is usually carried out in laminar drop tube (DTR) or entrained flow reactors (EFR). Typical experiments of this type have been conducted at Sandia National Laboratories [1,2], by Levendis et al. [3,4] or Joutsenoja et al. [5]. Imaging two-color pyrometry has been introduced in the late 1990s[6], when intensified (I)CCD-cameras with matching properties became available, which provide sufficient sensitivity for the detection of radiation on pf-particles in-flight, meaning short exposure times and thus little intensity.

Both detector types have been used to investigate different phenomena, e.g. the influence of the fuel rank[2,7], influence of enriched CO_2 concentrations [2,8,9](oxy-fuel combustion) and different questions on reaction models including effects like gasification reactions[10,11].

The performance of both detector types was compared in [12]. The results indicate that both approaches are on a comparable level and can be used for burning rate determination of pulverized coal. The spatial resolution of ICCD cameras was used to combine the measurement of particle temperature and particle shape of burning biomass particles in [13], showing that the burning rate analysis of biomass particles can gain significant advantages when the shape of burning particles is considered in the calculations, although this work only used a camera system with one viewing direction, measuring only the projection of the particle shape in the focal plane.

In order to measure the particle shape of burning biomass particles, a stereoscopic camera system has been developed, which is an upgrade of the system described in [8,12,13]. Its advantages are higher sensitivity, larger field of view, higher imaging frequency and, which is the major point, two viewing directions onto burning particles. The latter point not only creates the potential to detect the particle shape in terms of the particles outline, but also enables to measure the spatial position of the particle, which is necessary to prove the coincidence of particle position and focal plane.

The pyrometer was tested with one coal and one biomass sample, both burned in an O_2/N_2 dominated atmosphere. The measurements illustrate the systems capabilities and its working principle, highlighting future possibilities and the necessity of this analysis method.

Experimental Setup

The experiments were carried out in a flat flame burner (FFB), which is a laminar reactor providing typical conditions for pf-combustion. The burner is realized by a ceramics honeycomb (guiding the oxidizer) with approx. 200 hypodermic tubes (guiding CH_4 as fuel) equally distributed over the burner surface. Mass flow controllers are used to adjust the mixture of $CH_4/N_2/O_2/CO_2$. For the present experiments, an atmosphere containing 20% O_2, 11.5% CO_2 and 23% H_2O (volumetric, N_2 as balance, T_g= 1560 K) was chosen to avoid transport limitations of oxygen. The burner tube consists of quartz glass to provide optical access (inner diameter~ 65 mm). Particles are injected at the reactor center line with a small carrier gas flow (N_2) at low particle feed rates to avoid particle-to-particle interactions.

*Corresponding author: schiemann@leat.rub.de

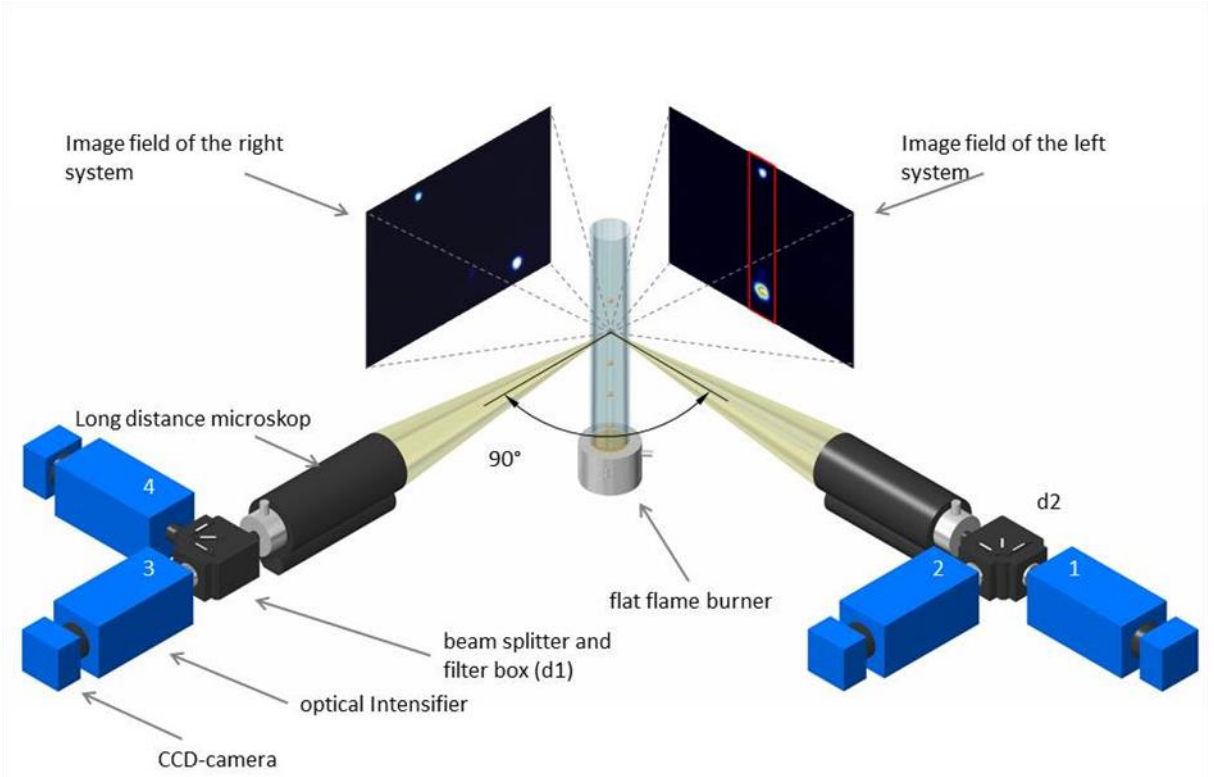

Figure 1: Schematic drawing of the camera-burner setup. The four cameras and two beam splitters are marked. The image field of the left camera branch bears a red rectangle, indicating the position of the well-focused particles recorded with the right camera branch.

The stereoscopic pyrometer SCOT (Stereoscopic Camera system for Optical Thermography) is depicted in Figure 1. It consists of four ICCD cameras (LaVision GmbH, Göttingen, Germany), two Questar long range microscopes and additional beam splitters (dichroic mirrors) and color filters (650±50 nm, 785±31 nm). It provides short exposure times in the range of microseconds and high sensitivity to detect particles in flight. Its spatial resolution was set to 6.8 µm/px, which is sufficient for typical particle sizes in pf experiments (40 µm and higher). A more detailed description of burner and camera system is given in [14].

Temperature and shape analysis

Particle temperature determination was carried out following the principle of two-color pyrometry using calibration curves. Cameras 1 and 2 were used to measure intensities of a black body of given temperature the two wave length bands in the temperature range from 1273-2473 K. From these measurements, calibration curves for several intensifier settings and exposure times were derived. For the present work, burning biomass particles were recorded with an exposure time of 5 µs. Post processing was carried out

$$d_{1/2} = 2k_{px}\sqrt{\frac{N_{1/2}}{\pi}}, \qquad (3)$$

to identify particles as zones of connected pixels with intensities above the background intensity (typically 3-4 counts, max. counts= 4095). The second criterion for particle identification was the position of burning particles, which had two fulfil the image position criterion mentioned in Figure 1 for minimized defocussing caused by depth-of-field effects. From the identified particles, the parameters L and d (interpreted as major and minor axes of a prolate ellipsoid) were calculated as outlined in Figure 2. The particle aspect ratio and its dimensions are described by

$$\frac{L}{d} = \frac{\sqrt{x_{1/2}^2 + x_{3/4}^2 + y_{3/4}^2}}{\frac{2}{\pi}\sqrt{\frac{N_{1/2}^2}{\sqrt{x_{1/2}^2 + y_{1/2}^2}} + \frac{N_{3/4}^2}{\sqrt{x_{3/4}^2 + y_{3/4}^2}}}}, \qquad (1)$$

where x denotes the horizontal extend of a particle projection, y means the vertical extend and N is the sum of all pixels with an intensity above the threshold. The indizes ½ and ¾ denote the two camera branches.

The particle diameter is calculated as

$$d = k_{px}\frac{2}{\pi}\sqrt{\frac{N_{1/2}^2}{\sqrt{x_{1/2}^2 + y_{1/2}^2}} + \frac{N_{3/4}^2}{\sqrt{x_{3/4}^2 + y_{3/4}^2}}}, \qquad (2)$$

where k_{px} is the pixel size in µm (calibrated with an precisely edged grid). Alternatively, for spherical particles the projected surface-equivalent particle diameter $d_{1/2}$ can be calculated as

which calculates the diameter projected to cameras 1 and 2 under the assumption of a spherical particle[12]. Furthermore, this representation makes the diameter comparable to the diameter measurement with non-imaging pyrometer devices.

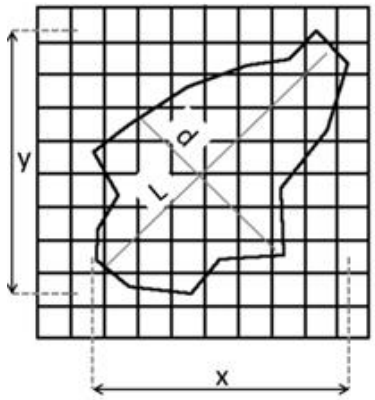

Figure 2: particle shape detection for a non-spherical particle based on its horizontal and vertical extend

Burning rate calculation

The burning rate of pulverized fuel particles is typically calculated by solving the energy balance around single burning particles [2,13,15]:

$$q\Delta H = \sigma\varepsilon\left(T_p^4 - T_w^4\right) + \frac{Nu\,\lambda}{d_{char}}\left(T_p - T_g\right) + \left(V_p/A_s\right)\rho_p c_p v_p \, {dT_p}/{dz} \quad (4)$$

The burning rate q [mol m^{-2} s^{-1}] is the desired value, which determines the heat release by chemical reaction when multiplied with the heat of reaction ΔH(neglecting CO_2 formation, only CO was considered, justified by the dominance of CO formation under the given conditions). The radiative heat flux is calculated from the Stefan-Boltzmann constant σ, the char emissivity ε (set to 0.8 in the following) and particle (T_p) and wall temperature (T_w). Although a more detailed description of the convective heat flux is available considering Stephan-Flow [17], this effect is neglected here, as it has no major influence under present conditions[17]. As the Nusselt-number is particle shape dependent, the relation

$$Nu = \frac{\alpha A}{\lambda}\frac{d_{char}}{A} \quad (5)$$

was used with the shape coefficient

$$\frac{\alpha A}{\lambda} = \frac{2\pi d\sqrt{\left({L}/{d}\right)^2 - 1}}{ln\left({L}/{d} + \sqrt{\left({L}/{d}\right)^2 - 1}\right)}. \quad (6)$$ [18]

The inert part was neglected, as it is typically very small compared to all other terms in eqn. (4). Therfore, dT_p/dz was set to 0[12,14]. The transport properties of the particle boundary layer were calculated using the single film model. A more detailed description can be found in [13].

Fuel preparation

Herbaceous biomass has a clear tendency to form fibrous particles with large aspect ratios. A Miscanthus sample was chosen as biomass fuel. The material was torrefied in a batch oven at 275°C for 30 min to adapt its properties on pf combustion needs, as is often suggested in literature [19]. The torrefied material was ground and sieved to a sieve size distribution of 90-125 µm. The proximate and ultimate analysis of the torrefied material show the following result:volatiles: 77.5%$_{waf}$, ash: 2.6%$_{wf}$, C: 51.4%$_{waf}$, H: 0.4%$_{waf}$, N: 5.8%$_{waf}$, S: 0.4%$_{waf}$, LHV: 20.3 MJ/kg. The sample was analyzed for its shape (L/d ratio) using an optical microscope (Zeiss Axiophot). The L/d ratio of nearly 1000 particles was measured to determine the initial aspect ratio distribution, which is shown in Figure 3. The results show, that the center of gravity of the aspect ratio distribution is between two and three, with $\overline{L/d} = 3.2$.

Experimental results

The results of particle L and d measurements at a position 120 mm behind the particle inlet, where volatile combustion had clearly finished, are shown in Figure 4. The particles have an average L/d of 2.68, and

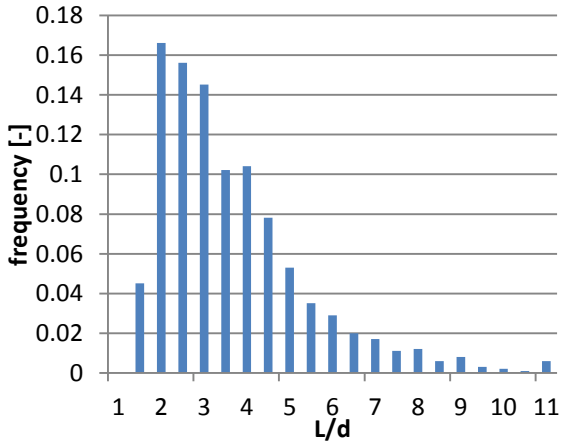

Figure 3: frequency of observed L/d ratios of the initial torrefied Miscanthus

the average minor half axis is 65.6 µm, which is below the minimum sieve size of 90 µm, but as biomass particles do not predominantly undergo swelling[20], and a certain burnout has to be considered, this appears acceptable. The L/d ratio ranges from 1.9 to 3.9, which is in general agreement with the L/d distribution depicted in Figure 3. It has to be mentioned, that the aspect ratio is larger than in the work mentioned before[13], which can be caused by the fuel type on the one hand, and the application of a stereoscopic technique in the present work on the other hand. Furthermore, the aspect ratio is slightly smaller for the burning particles than for the initial material, which

possible results from extended carbon consumption at the particle ends, but a certain overlap does exist.

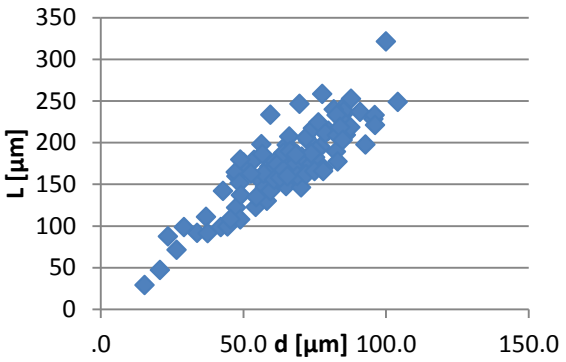

Figure 4: Measured particle L and d values for a fixed position in the particle streak.

Particle temperature was in a very narrow range and did not depend on particle diameter significantly, as is shown in Figure 5. The average temperature is T_{avg}= 2128 K, the standard deviation is σ_T= 132 K. It has to be noted, that the number of particles below the confidence interval $\bar{T} \pm \sigma_T$ exceeds the number of particles above the upper limit, which is a possible consequence of increased burn out leading to reduced reaction rates. Therefore, the deviation to higher temperatures is supposed to be slightly smaller than for low temperature events.

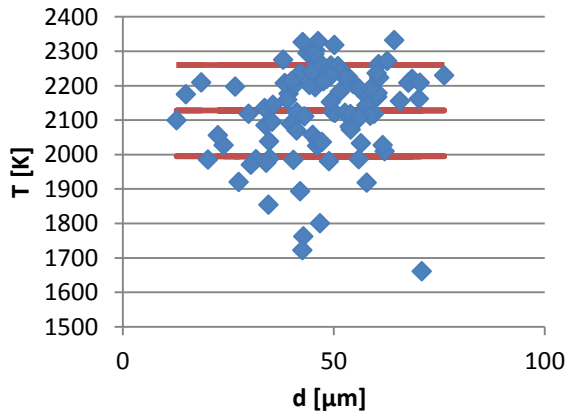

Figure 5: particle temperature plotted against the minor axis d, the horizontal lines denote T_{avg}-σ_T, T_{avg} and T_{avg}+σ_T from bottom to top.

The data was used to calculate particle burning rates. The calculation was carried out twice. Once, the particle shape was considered using the aspect ratio and shape factor, in a second calculation the burning rate was calculated using $d_{1/2}$ simulating a non-imaging detector with monoscopic view. The burning rates q (ellipsoid) and q (sphere) are depicted in Figure 6. The burning rates appear to be slightly larger for ellipsoidal particles, with a tendency to an average of 18.4 mol m^{-2} s^{-1} assuming spherical particles and 19.4 mol m^{-2} s^{-1}, when the ellipsoidal shape of biomass particles is considered.

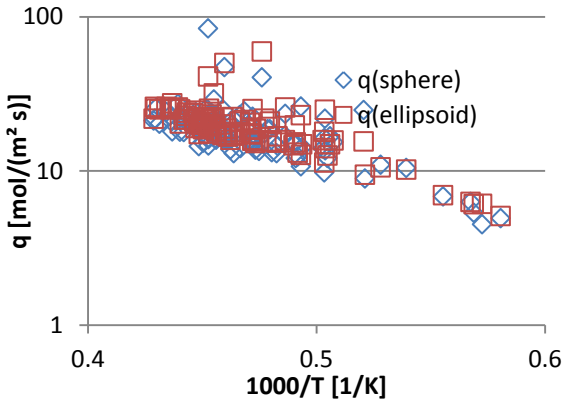

Figure 6: Burning rates under the assumption of spherical and ellipsoidal particle shape.

To point out the effect more clearly, the ratio $q_{sphere}/q_{ellipsoid}$ of particle burning rates was calculated for each particle in the data set. The result is shown in Figure 7. In average, the burning rate under the assumption of spherical geometry is 6% lower compared to the approach of considered spherical particle shape. The 2σ confidence interval

$$\frac{\overline{q_{sphere}}}{q_{ellipsoid}} \pm 2\frac{\sigma_n}{\sqrt{n}} = 0.94 \pm 0.032, \qquad (7)$$

shows, that the effect of neglected spherical particle shape is clearly demonstrated. The burning rate ratio of two particles clearly deviates from this tendency with $q_{sphere}/q_{ellipsoid} > 1.5$. It has been found, that the projected diameter $d_{1/2}$, which was used for the burning rate determination considering spherical particle shape (monoscopic view), was only 20 to 25% larger than the minor half axis d of the ellipsoidal particle dimensions,

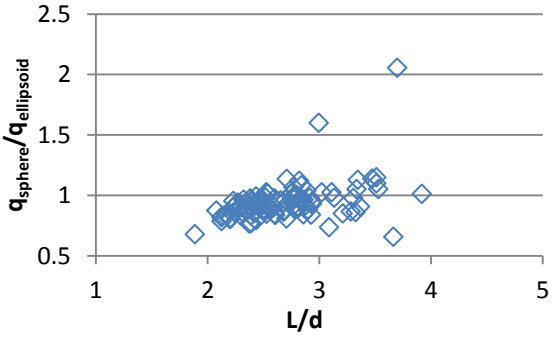

Figure 7: Ratio of calculated burning rates under the assumption of spherical and ellipsoidal shape.

but these particles were considerably smaller ($d_{1/2}$= 17 µm and 30 µm, d= 23 mm and 36 µm, L= 87.4 mm and 110.7 µm) than the average particle size. Note, that a detailed discussion on the effects of different L/d ratios and diameters determined as projected surface-equivalent diameters $d_{1/2}$ is given in[13].

The average derived from the data used for Figure 7 shows only a minor tendency to deviations in calculated burning rates under consideration of particle shape. A further step was taken, as the particle cloud was divided into particles above and below $d_{1/2}$= 100 µm. The resulting average L/d and $q_{sphere}/q_{ellipsoid}$ were plotted in

Figure 8. Although the smaller particles with an average $d_{1/2}$= 73 µm have an L/d~2.8, the burning rate ratio is almost unity. For larger particles (average $d_{1/2}$= 130 µm), the average L/d is only slightly smaller (2.6), but the burning rate ratio decreases to 0.89.

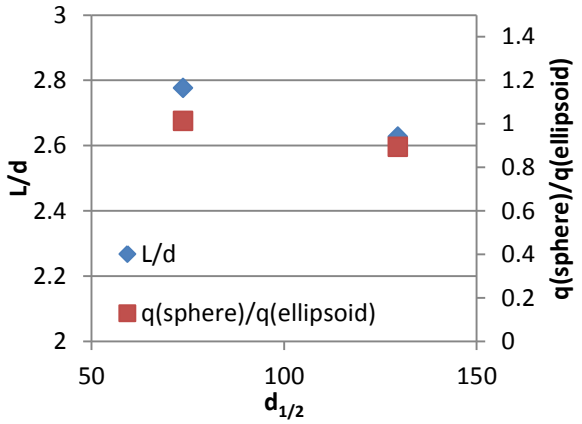

Figure 8: L/d and burning rate ratios depending on $d_{1/2}$

Discussion

The burning rates determined from the model for ellipsoidal particles show a clear tendency to reduced burning rates. Compared to the data presented in [13], the application of stereoscopic camera system provides slightly larger L/d ratios, and thus the effect of pseudo-3d particle shapes on the calculation of char burning rates becomes slightly more pronounced. The aspect ratio distributions measured before the combustion experiment and of burning particles show a decreasing tendency, which can be contributed to enhanced carbon consumption at the particle ends.

The data presented does not include calculation of rate parameters, e.g. to calculate char burning rates as Arrhenius type expression [12–14]. To calculate parameters for the typical Arrhenius expression of the oxidation reaction

$$q = A_o p_{O_2,s}^n e^{\left(-\frac{E_a}{RT_p}\right)}, \qquad (8)$$

the calculation of the oxygen partial pressure at the particle surface has to be included in future work.

Conclusions

A new stereoscopic imaging pyrometer system has been set up for the investigation of char burning kinetics under consideration of particle shape effects. Based on the measurement on particle temperature and assuming ellipsoidal shape for biomass particles, the energy balance around burning particles is solved to calculate the char burning rate.

As the initial results show, the system is capable of particle shape determination and simultaneous temperature measurement of single burning particles in a laminar entrained flow reactor.

The measured data were used to calculate the shape-dependent burning rate of single burning biomass char particles. A clear difference between the assumption of spherical and ellipsoidal particles was determined, with a trend to reduced burning rates in the case of assumed spherical particles with diameter determination from the projection surface in a monoscopic view.

The results indicate that for increased particle dimensions the aspect ratio analyses becomes increasingly important. This is in agreement with theoretical considerations from literature[13], which predicted this behavior.

Acknowledgement

This work has been financed by the German Research Foundation (DFG) within the project SCHI 1272/1-1.

References

[1] D.A. Tichenor, R.E. Mitchell, K.R. Hencken, and S. Niksa, Proc. Combust. Inst. **20**, 1213 (1985).

[2] J. Murphy and C. Shaddix, Combust. Flame **144**, 710 (2006).

[3] Y.A. Levendis, K.R. Estrada, and H.C. Hottel, Rev. Sci. Instrum. **63**, 3608 (1992).

[4] P.A. Bejarano and Y.A. Levendis, Combust. Flame **153**, 270 (2008).

[5] T. Joutsenoja, J. Saastamoinen, M. Aho, and R. Hernberg, Energy Fuels **13**, 130 (1999).

[6] G. Hackert, S. Wirtz, and H. Kremer, 9th Int. Symp. Appl. Laser Tech. to Fluid Mech. (1998).

[7] J. Riaza, R. Khatami, Y.A. Levendis, L. Álvarez, M. V. Gil, C. Pevida, F. Rubiera, and J.J. Pis, Combust. Flame **161**, 1096 (2014).

[8] M. Schiemann, V. Scherer, and S. Wirtz, Chem. Eng. Technol. **32**, 2000 (2009).

[9] P.A. Bejarano and Y.A. Levendis, Combust. Sci. Technol. **179**, 1569 (2007).

[10] E.S. Hecht, C.R. Shaddix, M. Geier, A. Molina, and B.S. Haynes, Combust. Flame **159**, 3437 (2012).

[11] M. Geier, C.R. Shaddix, K. Davis, and H.-S. Shim, Appl. Energy **93**, 675 (2012).

[12] M. Schiemann, M. Geier, C.R. Shaddix, N. Vorobiev, and V. Scherer, Rev. Sci. Instrum. **85**, 075114 (2014).

[13] M. Schiemann, S. Haarmann, and N. Vorobiev, Fuel **134**, 53 (2014).

[14] M. Schiemann, N. Vorobiev, and V. Scherer, Appl. Opt. **accepted**, (2015).

[15] R. Mitchell, Combust. Sci. Technol. **53**, 165 (1987).

[16] L. Tognotti, J. Longwell, and A. Sarofim, in *Symp. Combust.* (1991), pp. 1207–1213.

[17] J. Murphy and C. Shaddix, Sandia-Report 2003-8720J (2003).

[18] A. Wadewitz and E. Specht, Int. J. Heat Mass Transf. **44**, 967 (2001).

[19] D. Ciolkosz and R. Wallace, Biofuels, Bioprod. Biorefining **5**, 317 (2011).

[20] E. Cetin, B. Moghtaderi, R. Gupta, and T.. Wall, Fuel **83**, 2139 (2004).